

Lattice constants and magnetism of $L1_0$ -ordered FePt under high pressure

S. Sawada,¹ K. Okai,^{1,2} H. Fukui,^{1,2} R. Takahashi,¹ N. Ishimatsu,³ H. Maruyama,³ N. Kawamura,²
S. Kawaguchi,² N. Hirao,² T. Seki,^{4,5} K. Takanashi,^{4,5,6} S. Ohmura,⁷ and H. Wadati^{1,8,*}

¹*Department of Material Science, Graduate School of Science,
University of Hyogo, Ako-gun, Hyogo 678-1297, Japan*

²*Japan Synchrotron Radiation Research Institute, Sayo, Hyogo 679-5198, Japan.*

³*Graduate School of Advanced Science and Engineering,
Hiroshima University, Higashihiroshima, Hiroshima 739-8526, Japan*

⁴*Institute for Materials Research, Tohoku University, Sendai, Miyagi 980-8577, Japan*

⁵*Center for Spintronics Research Network, Tohoku University, Sendai, Miyagi 980-8577, Japan*

⁶*Center for Science and Innovation in Spintronics,
Tohoku University, Sendai, Miyagi 980-8577, Japan*

⁷*Faculty of Engineering, Hiroshima Institute of Technology, Hiroshima, Hiroshima 731-5193, Japan*

⁸*Institute of Laser Engineering, Osaka University, Suita, Osaka 565-0871, Japan*

We studied the relationship between the lattice constant and magnetism of $L1_0$ -ordered FePt under high pressure by means of first-principles calculations and synchrotron x-ray measurements. Based on our calculations, we found that the c/a ratio shows an anomaly at ~ 20 GPa and that the Pt magnetic moment is sharply suppressed at ~ 60 GPa. As for the c/a , we experimentally verified the anomaly at ~ 20 GPa by powder x-ray diffraction. We also measured the x-ray magnetic circular dichroism at the Pt L edge up to ~ 20 GPa. Any significant change of the Pt magnetic moment was not observed, in agreement with the calculations. These results thus indicate the possibility that novel magnetic states can be created in $L1_0$ -ordered FePt by lattice deformation under high pressure.

I. INTRODUCTION

With the advent of a Super Smart Society, the amount of information which we need to handle in our daily life is rapidly increasing. For the storage of large amounts of data, there has been a lot of interest in recording technology with magnetic materials. In order to achieve an efficient way of magnetic recording, ferromagnets with a strong magneto-crystalline anisotropy (MCA) are highly desired. $L1_0$ -ordered FePt has been intensively investigated due to its excellent chemical stability and strong uniaxial magnetic anisotropy (K_u) up to $\sim 7 \times 10^6$ J/m³ [1–4]. It is thus expected that this material will act as the next-generation magnetic recording devices.

At ambient pressure, the magnetism of FePt has been extensively studied by first-principles calculations and experiments [5–8]. From the first-principles calculations, it was found that the strong MCA in $L1_0$ FePt is due to the strong spin-orbit coupling (SOC) in the Pt $5d$ orbitals, and that the Pt atoms show ferromagnetism by the hybridization between the Fe $3d$ and Pt $5d$ states [5]. Ikeda *et al.* performed x-ray magnetic circular dichroism (XMCD) measurements of $L1_0$ -ordered FePt thin films and determined the magnetic moments of Fe $3d$ and Pt $5d$ states [8].

However, it is unknown how the lattice constants and magnetism change in $L1_0$ FePt under high pressure. Ko *et al.* determined the change of the unit-cell volume up to ~ 55 GPa by performing synchrotron radiation powder

X-ray diffraction (XRD) measurements of FePt alloys. They fitted the third-order Birch Murnaghan equation of state (BM-EOS) [9, 10] to the experimental data and obtained the parameters of $K_0 = 264.1$ GPa, $K' = 5.0$, and $V_0 = 26.74$ Å³ [11], where K_0 is a reference bulk modulus, K' is its pressure derivative, and V_0 is a reference volume. In their work, the behaviors of the lattice constants a and c were not given and the degree of the $L1_0$ ordering parameter of the studied sample was not clear.

In the present work, we studied the pressure effect of the lattice constants and magnetism of $L1_0$ -ordered FePt through both first-principles calculations and synchrotron x-ray measurements. In the calculations, we simulated the lattice constants a and c and unit-cell volume as a function of pressure. Specifically, the c/a ratio shows an anomaly at ~ 20 GPa. Moreover, the Pt magnetic moment is sharply decreased at ~ 60 GPa. In order to experimentally verify these anomalous behaviors indicated by the calculations, we performed measurements of powder XRD and XMCD under high pressure. We observed the c/a anomaly at ~ 20 GPa and almost no pressure dependence of the XMCD intensity up to ~ 20 GPa. These results will open a door to controlling magnetic states in $L1_0$ -ordered FePt by applying lattice deformation under high pressure.

II. CALCULATION

We performed first-principles calculations by using the Quantum ESPRESSO package [12, 13] with a projector augmented wave (PAW) method [14] within the general-

* wadati@sci.u-hyogo.ac.jp

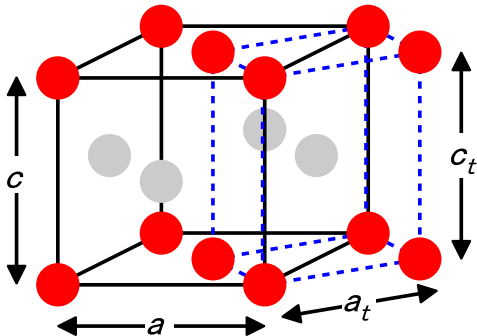


FIG. 1. The $L1_0$ crystal structure of FePt. The red (dark) and gray (light) spheres represent Fe and Pt atoms, respectively. The solid lines represent the fcc-like unit cell. The dashed lines represent the primitive cell used for first-principles calculations.

ized gradient approximation (GGA) of the density functional theory. We used a k -point sampling of $24 \times 24 \times 24$ with Monkhorst-Pack integration scheme [15] and energy cutoff of 280 Ry for one self-consistent field cycle.

Figure 1 shows the $L1_0$ crystal structure of FePt, where the solid lines represent the fcc-like unit cell and the dashed lines represent the primitive cell used for first-principles calculations. The $L1_0$ structure consists of alternating layers of Fe and Pt atoms along the (001) directions. The lattice parameters a_t and c_t for calculations are related to the fcc-like a and c as $a_t = a/\sqrt{2}$ and $c_t = c$. With fixing the unit cell volume, we searched for the minimum energy by varying a_t and c_t . The pressure is estimated based on the mean of the three diagonal components of the stress tensor.

We took spin polarization into account, and performed calculations in the presence and absence of SOC to investigate the effects of SOC on lattice constants and magnetism. In the absence of SOC, the valence electrons were Fe: $3s^2 3p^6 4s^2 3d^6$ and Pt: $5s^2 5p^6 5d^9 6s^1$, and the c/a ratio step was set to 0.0005. In the presence of SOC, the valence electrons were Fe: $3s^2 3p^6 4s^2 3d^6$ and Pt: $5s^2 5p^6 4f^{14} 5d^9 6s^1$, and the c/a ratio step was set to 0.0001.

III. EXPERIMENT

The FePt bulk samples for XRD measurements were sintered at 1000 °C for 24 hours. Then the sample was cut into a plate shape with $5 \times 5 \times 0.5$ mm³ through the wet processing. The crystal structure was characterized with laboratory XRD (Cu $K\alpha$ line).

We performed XRD and XMCD measurements at the SPring-8 beamlines BL10XU [16] and BL39XU, respectively. All the measurements were carried out at room temperature.

The experimental conditions of XRD were as follows:

x-ray wavelength of 0.4133 Å (the corresponding photon energy is 30 keV), no oscillation, and the exposure time of 5 seconds. We used a diamond-anvil cell with metallic rhenium gaskets to apply pressure to the sample. The culet size of the diamonds was 0.2 mm. In the sample chamber, we placed KCl, FePt, and KCl in this order. Powder XRD patterns were collected with the RIGAKU R-Axis IV⁺⁺ image-plate detector. The pressure was quantitatively estimated based on the pressure-volume relationship of KCl reported in Ref. [17].

The XMCD signals were collected by measuring the spectra of X-ray absorption spectroscopy (XAS) with the helicity-reversal method. A diamond phase retarder was employed to produce the circularly polarized beam. Powder FePt was annealed at 950 °C for 84 hours for the XMCD measurements. The obtained powder sample was sieved with a 25 μm mesh, and the fine powder was loaded into a hole of the gasket by using methanol:ethanol (= 4:1 ratio) solutions. The culet size of the diamonds was 0.45 mm, and nonmagnetic stainless steel (SU316L) gaskets were used to apply pressure to the sample. In order to magnetically saturate the sample, a high magnetic field of ±10 T was applied to the $L1_0$ -FePt powder. We designed a miniature diamond anvil cell to be accommodated in the small sample chamber of the superconducting magnet (25 mm in diameter). The pressure in the sample cavity was monitored by using the conventional method of ruby fluorescence measurements [18].

IV. RESULTS AND DISCUSSIONS

Figure 2 shows the pressure dependence of the lattice constants (a and c), the c/a ratio, and the primitive-cell volume ($V = a^2 c/2$) obtained from the first-principles calculations, where the results both with and without SOC are shown. The lattice constants a and c decreased monotonically by the application of pressure, whereas the c/a ratio showed non-monotonic behaviors, namely a local maximum at ~ 10 GPa with SOC and at ~ 20 GPa without SOC. We fitted the following BM-EOS to the obtained data

$$P(V) = \frac{3K_0}{2}(\eta^{-7} - \eta^{-5})[1 + \frac{3}{4}(K' - 4)(\eta^{-2} - 1)], \quad (1)$$

where $\eta = (V(P)/V_0)^{1/3}$, $(a(P)/a_0)$, or $(c(P)/c_0)$, and P is the pressure. The subscript 0 means the value at the ambient conditions. The obtained parameters were $K_0 = 210(3)$ GPa, $K' = 4.5(1)$, and $V_0 = 27.83(2)$ Å³ with SOC, and $K_0 = 210(4)$ GPa, $K' = 4.5(2)$, and $V_0 = 28.04(2)$ Å³ without SOC.

In order to investigate how the c/a anomaly seen in Fig. 2 affects magnetism, we plotted the magnetic moments of Fe and Pt as a function of pressure in Fig. 3. At ambient pressure, the magnetic moments of Fe and Pt were estimated to be 3.0 μ_B and 0.37 μ_B with SOC, in good agreement with the experimental values reported in

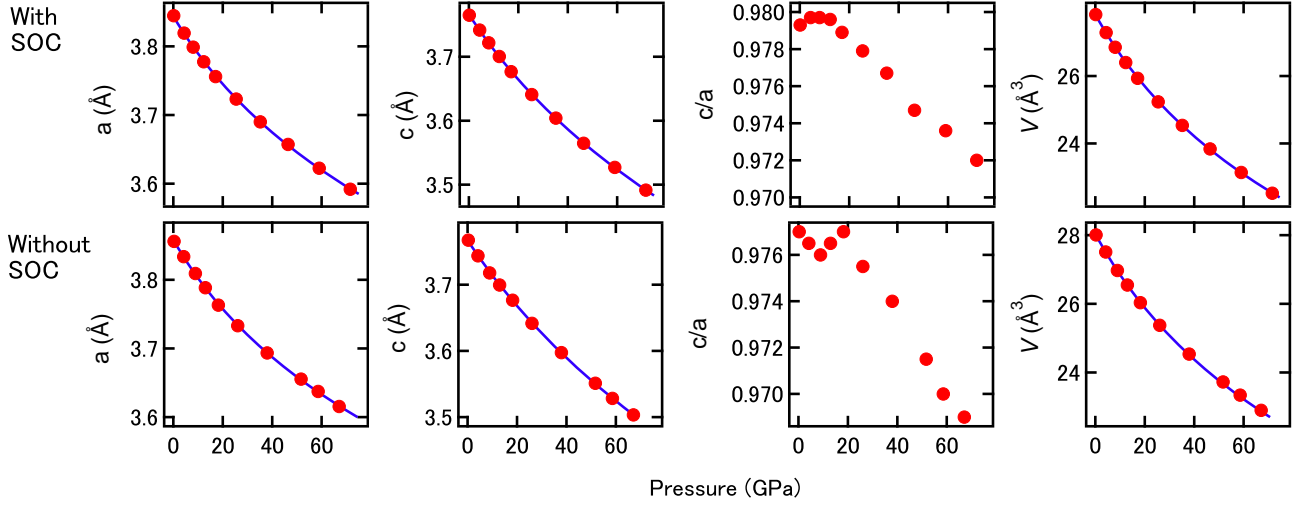


FIG. 2. Pressure dependence of lattice constants (a and c), the c/a ratio, and the primitive-cell volume (V) estimated by the first-principles calculations. The solid lines are the fitted curves of the third-order BM-EOS. The results with and without SOC are shown.

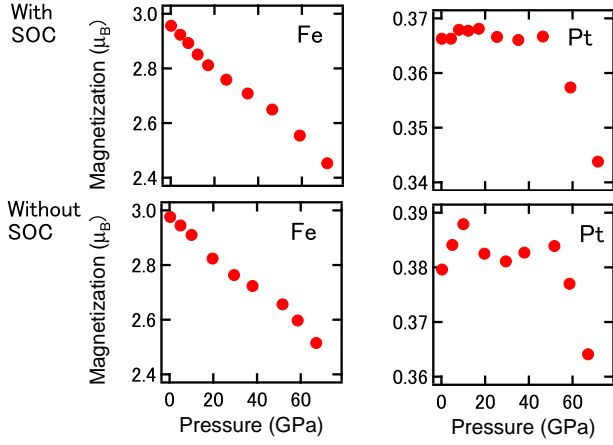


FIG. 3. Magnetic moments of Fe and Pt obtained by first-principles calculations under high pressure. The results with and without SOC are shown.

a prior XMCD study [8]. The Fe magnetic moment decreased monotonically with increasing pressure both with and without SOC. The slope of the decrease changes at ~ 20 GPa, where we found that the c/a ratio shows a local maximum from the calculations without SOC. The Pt magnetic moment was almost constant up to about 50 GPa with SOC and showed a local maximum at ~ 10 GPa without SOC. Despite the difference between the two cases seen in the low-pressure regime, the magnetic moment suddenly diminished above 50 GPa in both cases.

In the light of the pressure effects obtained by the first-principle calculations above, we aim to verify the obtained calculation results by performing x-ray measurements. First, we attempted to observe the c/a behav-

ior by powder XRD. Before applying high pressure, we characterized the FePt sample by using laboratory XRD. Figure 4 (a) shows a powder XRD pattern at ambient pressure. We observed the peaks corresponding to the following Miller indices: 001, 110, 111, 200, 002, 201, 112, 220, 202, 311, 222, and 312, mirroring the $L1_0$ -ordered structure. Based on this XRD pattern, the lattice constants were determined to be $a = 3.857$ Å and $c = 3.735$ Å, in good agreement with $a_t = 2.722$ Å and $c_t = 3.700$ Å reported in Ref. [19]. The degree of long-range chemical order S is defined as follows:

$$S = \frac{r_{Fe} - x_{Fe}}{y_{Fe}} = \frac{r_{Pt} - x_{Pt}}{y_{Pt}}, \quad (2)$$

where x_{el} , y_{el} , and r_{el} ($el = Fe, Pt$) are atomic fraction, fraction of the sites, and fraction of the sites occupied by the correct element, respectively. Based on the Rietveld analysis of the powder XRD pattern, we determined the value of S to be 0.67.

After these characterizations, we performed powder XRD measurements under high pressure. Figure 4 (b) shows the typical XRD patterns in the applications of pressure. The 200 and 110 peaks of KCl were observed at 0.1 GPa and at 22.8 GPa or more, respectively. This corresponds to the B1 to B2 phase transition of KCl at 2.6 GPa [17]. The pressure-independent XRD patterns of FePt indicate that the $L1_0$ -ordered crystal structure with $S = 0.67$ was kept up to 72.8 GPa. We converted XRD images into conventional XRD patterns by using IPAnalyzer and then determined the lattice constants a and c by using PDIndexer [20]. The obtained parameters a , c , c/a and V are listed in TABLE I, and plotted in Fig. 5. The lattice constants a and c monotonically decreased by applying pressure. We fitted BM-EOS to the experimental data and obtained the parameters $K_0 = 231(7)$

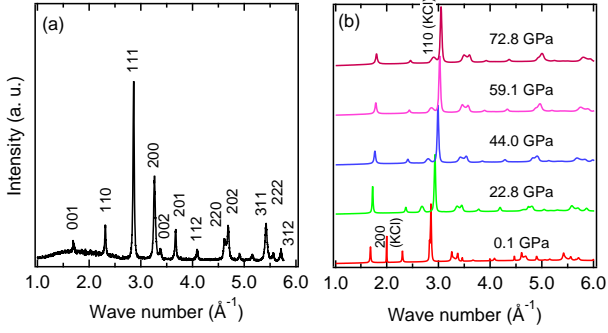


FIG. 4. Powder XRD patterns of FePt under ambient (a) and high pressure (b). In panel (b), the peaks of KCl were also observed. Indices in panel (b) are for KCl B1 (below 2.8 GPa) and B2 (above that) phases.

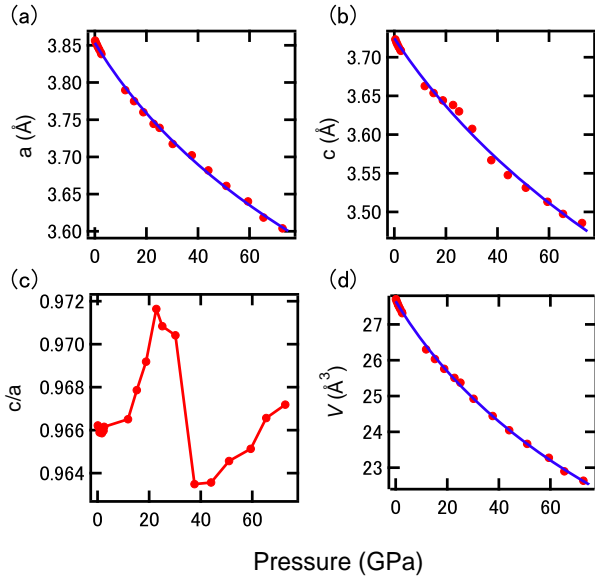


FIG. 5. Lattice constants (a and c), the c/a ratio, and the primitive-cell volume (V) obtained by powder XRD under high pressure. The solid lines are the fitted curves by the third-order BM-EOS.

GPa, $K' = 4.5(3)$, and $V_0 = 27.64(3) \text{ Å}^3$. Since there is no anomaly in V as a function of pressure, we used a single parameter set. The obtained Birch-Murnaghan parameters are listed in Table II, alongside the values obtained from our first-principles calculations above. The experimental value of V_0 is smaller than those of the calculations due to the tendency of GGA to systematically overestimate lattice constants [21]. The experimental K is larger than the calculated values because GGA underestimates bulk moduli [21]. The experimental value of c/a shows a maximum at 20 GPa, which is qualitatively in agreement with the calculation without SOC in Fig. 2.

We further attempted to observe the magnetic moment of Pt by high-pressure XMCD, as shown in Fig. 6. The inset shows the XAS and XMCD spectra at the Pt L_3

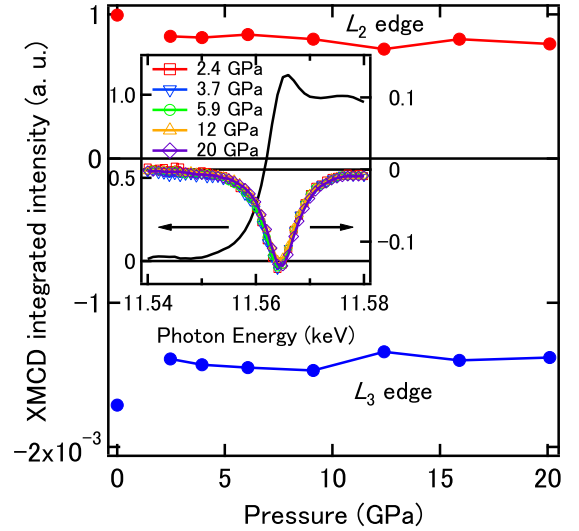


FIG. 6. The XMCD intensity at Pt L_3 and L_2 edges under high pressure. The inset shows the XAS (left axis) and XMCD (right axis) spectra at the Pt L_3 edge.

edge up to 20 GPa. One can see that the XMCD spectra are almost independent of pressure. The main panel shows the XMCD intensity at Pt L_3 and L_2 edges under high pressure. The intensity did not change by applying high pressure up to 20 GPa, indicating that the Pt magnetic moment is insensitive to pressure. The pressure-independent magnetic moment is consistent with the calculation in Fig. 3, in particular with SOC, where Pt magnetic moments are almost constant in the pressure regime of the present experiments. This strongly suggests that SOC should be taken into account in the calculation of magnetism. The sudden drop of the Pt magnetic moment, which we expect based on the first-principles calculations in Fig. 3, will be left for the future XMCD measurements under the pressure greater than 50 GPa.

In the present work, we studied the pressure dependence of the lattice constant and magnetism of $L1_0$ -ordered FePt by first-principles calculations. Moreover, in the powder XRD and XMCD experiments, we observed most of the quantities that we numerically calculated. The magnetic anisotropy of $L1_0$ -ordered FePt is considered to originate in SOC [8], and thus it can be expected that the magnetic properties can be controlled in the future by changing the lattice constants under high pressure.

V. SUMMARY

We studied the relationship between the lattice constant and magnetism of $L1_0$ -ordered FePt under high pressure by a combination of first-principles calculations and x-ray measurements. The calculations showed the c/a ratio anomaly at ~ 20 GPa, which was observed by

powder XRD under high pressure. We also measured the Pt magnetic moment by XMCD and found almost no pressure dependence, in agreement with the calculations. The XRD under higher pressure at ≥ 50 GPa is expected to reveal the decrease of the Pt magnetic moment. We successfully clarified the behavior of the lattice constants and magnetism in $L1_0$ -ordered FePt under high pressure, which will lead to the creation of new magnetism in these

materials.

ACKNOWLEDGMENT

We would like to thank S. Nakata for fruitful discussions. Measurements were performed with the approval of the Japan Synchrotron Radiation Research Institute (No. 2019B1623). This work was partially supported by JSPS KAKENHI to HW (JP19H05824) and to HF (JP19H02004).

-
- [1] O. A. Ovanov, L. V. Solina, and V. A. Demshina, *Phys. Met. Metallogr.* **35**, 81 (1973).
 - [2] T. Shima, K. Takanashi, Y. K. Takahashi, and H. Hono, *Appl. Phys. Lett.* **81**, 1050 (2002).
 - [3] T. Shima, K. Takanashi, Y. K. Takahashi, K. Hono, G. Q. Li, and S. Ishio, *J. Magn. Magn. Mater.* **266**, 171 (2003).
 - [4] J. Lyubina, I. Opahle, M. Richter, O. Gutfleisch, K.-H. Müller, L. Schultz, and O. Isnard, *Appl. Phys. Lett.* **89**, 032506 (2006).
 - [5] I. V. Solovyev, P. H. Dederichs, and I. Mertig, *Phys. Rev. B* **52**, 13419 (1995).
 - [6] Y. Kota and A. Sakuma, *J. Phys. Soc. Jpn.* **81**, 084705 (2012).
 - [7] S. Ueda, M. Mizuguchi, Y. Miura, J. G. Kang, M. Shirai, and K. Takanashi, *Appl. Phys. Lett.* **109**, 042404 (2016).
 - [8] K. Ikeda, T. Seki, G. Shibata, T. Kadono, K. Ishigami, Y. Takahashi, M. Horio, S. Sakamoto, Y. Nonaka, M. Sakamaki, K. Amemiya, N. Kawamura, M. Suzuki, K. Takanashi, and A. Fujimori, *Appl. Phys. Lett.* **111**, 142402 (2017).
 - [9] F. Birch, *J. Geophys. Res.* **57**, 227 (1952).
 - [10] F. D. Murnaghan, *Proc. Natl Acad. Sci. USA* **30**, 244 (1944).
 - [11] Y. H. Ko, K. J. Kim, C. K. Han, C. Petrovic, R. Hu, H. H. Lee, and Y. Lee, *High Press. Res.* **29**, 800 (2009).
 - [12] P. Giannozzi, S. Baroni, N. Bonini, M. Calandra, R. Car, C. Cavazzoni, D. Ceresoli, G. L. Chiarotti, M. Cococcioni, I. Dabo, *et al.*, *J. Phys: Condens. Matter* **21**, 395502 (2009).
 - [13] P. Giannozzi, O. Andreussi, T. Brumme, O. Bunau, M. B. Nardelli, M. Calandra, R. Car, C. Cavazzoni, D. Ceresoli, M. Cococcioni, *et al.*, *J. Phys: Condens. Matter* **29**, 465901 (2017).
 - [14] P. E. Blöchl, *Phys. Rev. B* **50**, 17953 (1994).
 - [15] H. J. Monkhorst and J. D. Pack, *Phys. Rev. B* **13**, 5188 (1976).
 - [16] N. Hirao, S. I. Kawaguchi, K. Hirose, K. Shimizu, E. Ohtani, and Y. Ohishi, *Matter. Radiat. Extremes* **5**, 018403 (2020).
 - [17] A. Dewaele, A. B. Belonoshko, G. Garbarino, F. Occelli, P. Bouvier, M. Hanfland, and M. Mezouar, *Phys. Rev. B* **85**, 214105 (2012).
 - [18] H. K. Mao, J. Xu, and P. M. Bell, *J. Geophys. Res.* **91**, 4673 (1986).
 - [19] S. Yuasa, H. Miyajima, and Y. Otani, *J. Phys. Soc. Jpn.* **63**, 3129 (1994).
 - [20] Y. Seto, D. Hamane, T. Nagai, and N. Sata, *Rev. High pressure Sci. Technol.* **20**, 269 (2010).
 - [21] G. I. Csonka, J. P. Perdew, A. Ruzsinszky, P. H. T. Philipsen, S. Lebegue, J. Paier, O. A. Vydrov, and J. G. Angyan, *Phys. Rev. B* **79**, 155107 (2009).

TABLE I. Lattice constants (a and c), the c/a ratio, and the primitive-cell volume (V) obtained by powder XRD under high pressure.

Pressure (GPa)	a (Å)	c (Å)	c/a	V (Å ³)
0.1	3.8563(3)	3.7261(5)	0.9662(1)	27.706(6)
0.4	3.8535(3)	3.7230(5)	0.9661(1)	27.642(6)
0.8	3.8507(6)	3.719(1)	0.9658(3)	27.57(1)
1.2	3.8476(8)	3.717(2)	0.9661(6)	27.51(2)
1.7	3.844(1)	3.713(2)	0.9659(6)	27.43(2)
2.3	3.840(1)	3.710(3)	0.9661(8)	27.35(3)
2.5	3.838(1)	3.708(2)	0.9661(6)	27.31(2)
11.8	3.790(1)	3.663(2)	0.9665(6)	26.31(2)
15.2	3.775(1)	3.654(2)	0.9679(6)	26.04(2)
18.8	3.7600(8)	3.644(2)	0.9691(6)	25.76(2)
22.8	3.744(1)	3.638(2)	0.9717(6)	25.50(2)
25.1	3.739(1)	3.630(2)	0.9708(6)	25.37(2)
30.2	3.717(1)	3.607(3)	0.9704(8)	24.92(2)
37.6	3.702(2)	3.567(3)	0.964(1)	24.44(3)
44.0	3.682(2)	3.548(3)	0.964(1)	24.05(3)
51.0	3.661(1)	3.531(3)	0.9645(9)	23.66(2)
59.4	3.640(2)	3.513(3)	0.965(1)	23.27(3)
65.4	3.618(1)	3.497(2)	0.9666(6)	22.89(2)
72.8	3.604(1)	3.486(2)	0.9673(6)	22.64(2)

TABLE II. Birch-Murnaghan equation-of-state parameters K_0 , K' , and V_0 obtained by fitting calculated and experimental results.

	K_0 (GPa)	K'	V_0 (Å ³)
Calc (with SOC)	210(3)	4.5(1)	27.83(2)
Calc (without SOC)	210(4)	4.5(2)	28.04(2)
Exp	231(7)	4.5(3)	27.64(3)